Journal of
Materials Chemistry A

Accepted Manuscript

This article can be cited before page numbers have been issued, to do this please use: Y. Wang, F. Cao, W. Lin, F. Zhao, J. Zhou, S. LI and G. W. Qin, *J. Mater. Chem. A*, 2019, DOI: 10.1039/C9TA04487F.

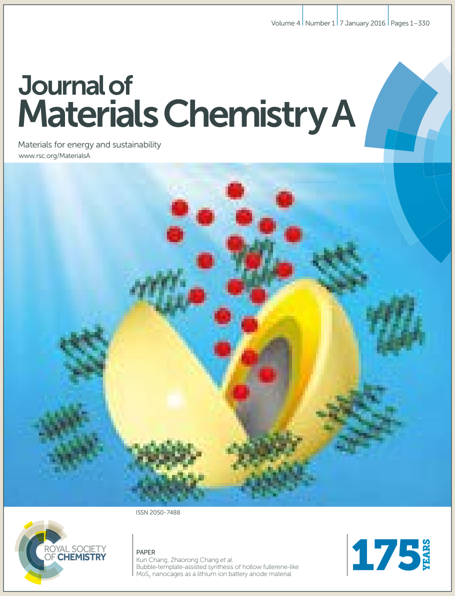

ROYAL SOCIETY OF CHEMISTRY

rsc.li/materials-a

View Article Online
DOI: 10.1039/C9TA04487F

Table of Contents Entry

In situ synthesis of Ni/NiO composites with defect ultrathin nanosheets for highly efficient biomass-derivatives selective hydrogenation

Yunan Wang[1], Feng Cao[*1], Weiwei Lin[*2, 3], Fengyu Zhao[2, 3], Jun Zhou[1], Song Li[*1], Gaowu Qin[1, 4]
[1]*Key Laboratory for Anisotropy and Texture of Materials (Ministry of Education), School of Material Science and Engineering, Northeastern University, Shenyang 110819, China*
[2]*State Key Laboratory of Electroanalytical Chemistry, Changchun Institute of Applied Chemistry, Chinese Academy of Sciences, Changchun 130022, P. R. China*
[3]*Jilin Province Key Laboratory of Green Chemistry and Process, Changchun Institute of Applied Chemistry, Chinese Academy of Sciences, Changchun 130022, P. R. China*

[*]*caof@atm.neu.edu.cn*
**linwei@ciac.ac.cn*
[*]*lis@atm.neu.edu.cn*

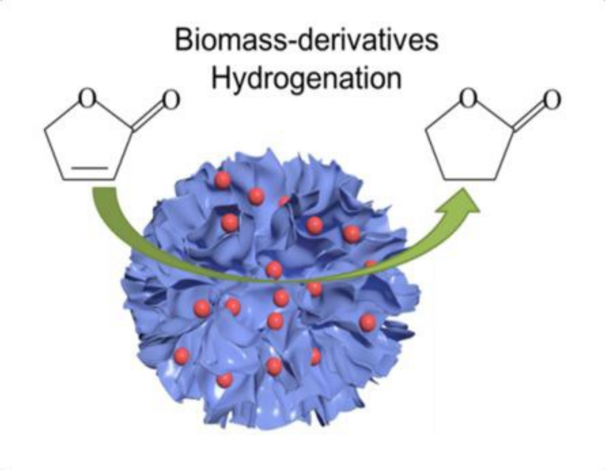

Synergism of geometric construction and electronic regulation: numerous Ni nanoparticles combined with defect-rich ultrathin NiO nanosheets for efficient hydrogenation.

View Article Online
DOI: 10.1039/C9TA04487F

Journal Name

ARTICLE

Received 00th January 20xx,
Accepted 00th January 20xx

DOI: 10.1039/x0xx00000x

www.rsc.org/

In situ synthesis of Ni/NiO composites with defect ultrathin nanosheets for highly efficient biomass-derivatives selective hydrogenation

Yunan Wang [a], Feng Cao*[a], Weiwei Lin*[b, c], Fengyu Zhao [b, c], Jun Zhou [a], Song Li *[a], Gaowu Qin [ad]

Herein, Ni/NiO composite catalyst was synthesized by a simple *in situ* reduction method, and its catalytic hydrogenation performance has been verified to be even superior to that of noble metals. In particular, the catalysts can transform 2(5H)-furanone (HFO) to γ-butyrolactone (GBL) efficiently under mild conditions, which can achieve the upgradation for biomass-derivatives. The superior catalytic activity can be attributed to the synergism of geometric construction and electronic regulation. Specifically, ultrathin NiO nanosheets contain plenty of surface defects and relatively large mesopores. Those defects can be helpful to the activation and dissociation of hydrogen, the adsorption of HFO molecules as well as the enhancement of local hydrogen concentration on catalysts, while the pores can be considered as nano-reactors for the hydrogenation. The strong interaction at the interface caused by *in situ* synthesis can further tune its electronic structures and improve the hydrogen adsorption. In addition, the catalyst also displays great catalytic properties for *p*-nitrophenol (PNP) hydrogenation and nonenzymatic glucose sensing, which further supports the promising application potential of such catalysts with the unique mesostructures of Ni/NiO heterojunctions with defect ultrathin nanosheets.

Introduction

Biomass is the only candidate for the sustainable carbon source to produce necessities for people. [1-3] Consequently, the upgradation of biomass-derived intermediate compounds is of vital importance to the manufacture of high-value products. [4,5] In particular, 2(5H)-furanone (HFO) is a common biomass derivative, and its molecular structure includes only one more C=C bond than γ-butyrolactone (GBL), making it a potential platform compound to produce GBL. [6] GBL is an important organic intermediate in the area of fine chemicals synthesis, medicines, pesticides and spices.[7-9] However, the simultaneous hydrogenation of C=O bond and the ring opening via C-O bond scission also largely increase the difficulty of HFO selective hydrogenation to GBL. [10] Currently, most catalysts used for the hydrogenation of HFO to GBL are noble metal-based catalysts due to their unique physical and chemical properties. For instance, a series of Pt-based composite catalysts have been prepared by Li *et al.* to apply to the hydrogenation of HFO. [11] However, the high cost and low reserves of noble metals can largely block their practical applications. Ni-based catalysts have been verified to possess excellent performance in various hydrogenation reactions due to their unique d-band structure, even comparable to most noble metals. [12-14] The performance can be further enhanced through the tuning of heterojunctions to metals. Therefore, Ni-based composite catalysts are considered to be promising materials for the selective hydrogenation of HFO to GBL through the tuning of heterojunctions to metals.

Almost all the ingenious tuning can be attributed to the geometric construction and electronic regulation. For the geometric construction, 2D ultrathin nanosheets have attracted increasing interest due to its unique physical and chemical properties. [15-17] In addition, the electronic regulation mainly includes defect tuning and interface tuning. Numerous defects can lead to the decrease of the metal coordination numbers of the surface atoms. [18] The smaller the metal coordination number is, the smaller the d band width and hence the higher the energy of the d band center can achieve, causing a stronger adsorption for H_2. [19] The strong adsorption can facilitate the dissociation and activation of H_2. Niu *et al.* have also found that oxygen vacancies can largely improve the performance of Fe_3O_4 in nitroarene hydrogenation by lowering the energy barrier of H_2 dissociating and activating. [20] Meanwhile, the strong interaction at the interface of heterojunctions is also widely believed to permit tuning of the

---

[a] *Key Laboratory for Anisotropy and Texture of Materials (Ministry of Education), School of Material Science and Engineering, Northeastern University, Shenyang 110819, China. Email: caof@atm.neu.edu.cn(F. Cao), lis@atm.neu.edu.cn (S. Li)*
[b] *State Key Laboratory of Electroanalytical Chemistry, Changchun Institute of Applied Chemistry, Chinese Academy of Sciences, Changchun 130022, P. R. China Email: linwei@ciac.ac.cn(W. W. Lin)*
[c] *Jilin Province Key Laboratory of Green Chemistry and Process, Changchun Institute of Applied Chemistry, Chinese Academy of Sciences, Changchun 130022, P. R. China*
[d] *Research Center for Metallic Wires, Northeastern University, Shenyang 110819, China.*

Electronic Supplementary Information (ESI) available: Experimental section; SEM and XRD of $Ni(OH)_2$ precursors; TEM, N_2 adsorption–desorption isotherms and water vapor adsorption isotherms for Ni/NiO composites. Characterizations and performance for Ni/NiO composite catalysts with thick nanosheets. Performance of catalytic PNP hydrogenation with Ni/NiO composite catalysts. Electrochemical sensing for glucose for Ni/NiO composites. See DOI: 10.1039/x0xx00000x

View Article Online
DOI: 10.1039/C9TA04487F

electronic structures of metals through the transfer of electrons at the intimate interface caused by the difference of work function. [21] Therefore, it is of great importance to obtain low-cost Ni-based composite catalysts to realize efficient HFO hydrogenation through the tuning of heterojunctions to metals.

Herein, highly active Ni/NiO composite catalysts with numerous Ni nanoparticles closely combined with the defect-rich and ultrathin NiO nanosheets were successfully prepared by a simple *in situ* reduction method. The catalysts exhibit a conversion rate of approximately 95.6% in 1 h and the selectivity of approximately 90.5% for HFO hydrogenation to GBL, which are superior to most reported catalysts, even noble metal catalysts.

Results and discussion

Properties of Ni/NiO catalysts: $Ni(OH)_2$ pure phase with 3D flower-like morphologies was prepared through a simple hydrothermal method, as shown in Fig. S1 and S2, the same as our previous studies. [22] The as-prepared $Ni(OH)_2$ was then calcined at 500 °C for 2 h and further reduced at different temperatures for 1 h by H_2. The obtained samples were characterized by X-ray diffraction patterns (XRD), as shown in Fig. 1. It is obvious that the pure NiO phase was achieved after calcination. Its low peak intensities indicate its poor crystallinity, which might be caused by its mesostructures with ultrathin nanosheets and abundant defects. Once reduced by H_2, the Ni phase appears. For the Ni/NiO-400, Ni/NiO-450 and Ni/NiO-500, there are no other phases appearing except for Ni and NiO, indicating that Ni/NiO composites were successfully synthesized. In addition, the average particle size of metallic Ni was calculated to be 11.1, 11.7 and 13.2 nm for Ni/NiO-400, Ni/NiO-450 and Ni/NiO-500, respectively, according to the Debye–Scherrer equation. Once the reduction temperature was increased to 550 °C, the NiO peaks disappeared and pure Ni was obtained.

Field emission scanning electron microscopy (FE-SEM) was then applied to observe the morphologies of the obtained samples after calcination and reduction, which is exhibited in Fig. 2. The morphology of pure NiO has not obviously changed compared with the $Ni(OH)_2$ precursor. For the Ni/NiO-400, Ni/NiO-450 and Ni/NiO-500, the flower-like structure is still maintained, without clear damage. However, the morphology of Ni/NiO-550 suffered complete destruction, and the reduced Ni nanoparticles seriously aggregate. Therefore, it is clear that NiO nanosheets can be helpful to protect Ni nanoparticles from aggregating at 400-500 ˚C.

To further understand the mesostructures of the obtained samples, transmission scanning electron microscopy (TEM) was employed. As shown in Figs. 3(a) and (b), pure NiO contains large amounts of ultrathin nanosheets with a thickness of approximately 2.5 nm, which is in agreement with the results of TEM shown in Fig. S3, further supported by the reports of Fan *et al*. [24] Once reduced by H_2, as shown in Figs. 3(c-e), Ni nanoparticles appear and form heterojunctions with NiO nanosheets. Figs. 3(f-h) show that the average diameter of Ni nanoparticles of the samples reduced at 400, 450 and 500 °C was approximately 11.5, 12 and 13 nm, respectively. The good thermal stability of the mesostructure can be ascribed to the strong interaction between Ni and NiO, caused by the *in situ* synthesis. [25] Additionally, it can be seen from Figs. S4(a) and (b) that Ni particles combined with NiO in the form of face to face for both Ni/NiO-450 and Ni/NiO-500, which leads to an intimate interface between metal nanoparticles and oxides, further verifying the unique advantages of *in situ* synthesis. Meanwhile, for Ni/NiO-500, resolved lattice fringes with interplanar distance of 0.202, 0.243 and 0.204 nm are observed through high-resolution transmission scanning electron microscope (HRTEM) analysis, corresponding to (111) planes of Ni as well as (111) and (200) planes of NiO, respectively, as shown in Fig. S5.

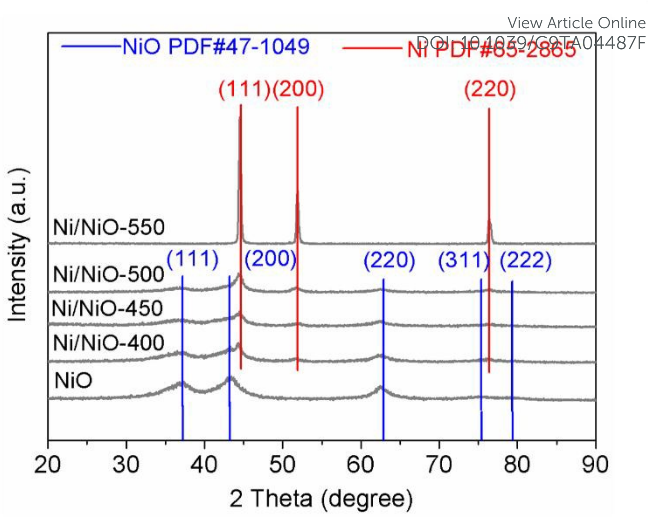

Fig. 1 XRD patterns of Ni/NiO composite catalysts reduced at different temperatures (400 – 550 ℃) for 1 h by H_2.

X-ray photoelectron spectroscopy (XPS) measurements were then applied to characterize the as-prepared samples. As shown in Fig. 4(a), for NiO, the chemical binding energies at approximately 854.8, 873.5, 856.8 and 875.3 eV can be due to Ni^{2+} 2p3/2, Ni^{2+} 2p1/2, Ni^{3+} 2p3/2 and Ni^{3+} 2p1/2 spin-orbit peaks, respectively, and the peaks at approximately 862.1 and 880.6 eV are the satellite shake-ups of the assigned components. [26] NiO, as a typical p-type semiconductor, usually contains large amounts of Ni^{2+} vacancies. To maintain a neutral charge near the Ni^{2+} vacancies, some of the neighboring Ni^{2+} ions transferring to Ni^{3+} through combining with the cation hole (h^+) left by the original Ni^{2+}, which is only considered as local charge balance without breaking the crystalline structure of NiO. [27-29] XPS measurements have also universally applied to confirm the existence of Ni^{3+}, whose characteristic peaks are believed to appear at a higher binding energy than those of Ni^{2+} in NiO.[30, 31] Meanwhile, the distribution and chemical states of the O element in pure NiO are exhibited in Fig. 4(d) and there are three fitted peaks in that spectra, O_I, O_{II} and O_{III}. The peak at the lowest binding energy of approximately 530.0 eV is characteristic of the lattice oxygen of NiO supports (O_I). [32] The peak at 531.5 eV is assigned to a high number of defect

View Article Online
DOI: 10.1039/C9TA04487F

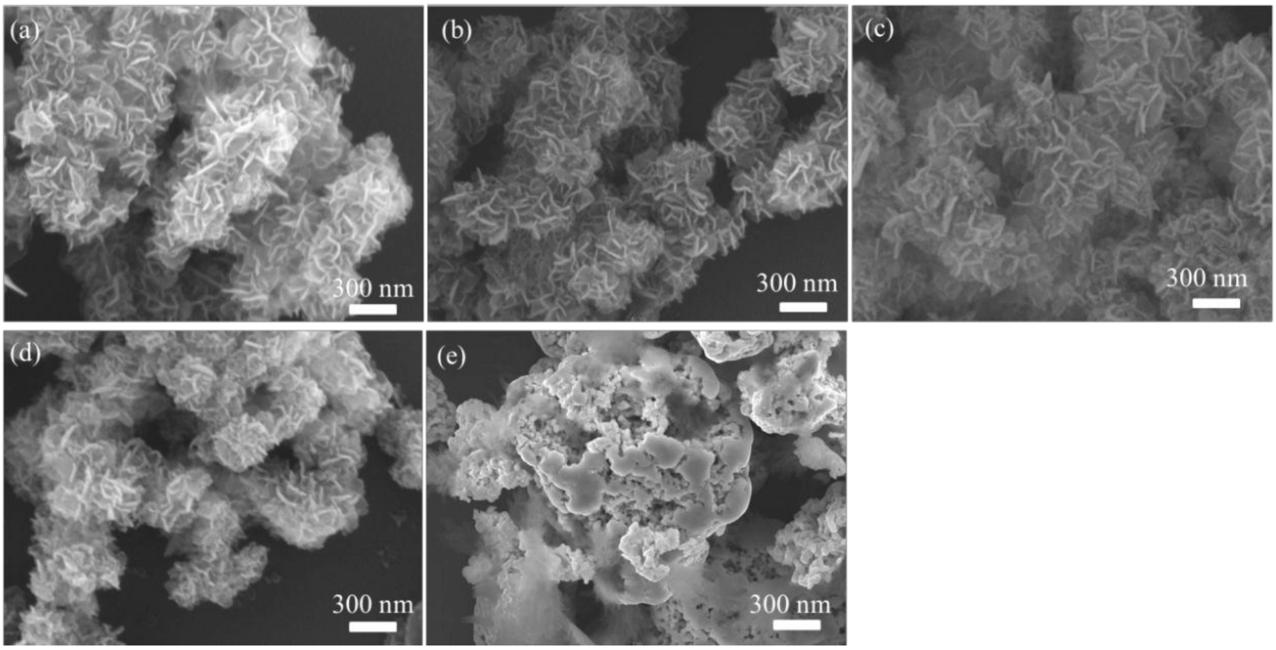

Fig. 2 SEM images of Ni/NiO composite catalysts (a) NiO, (b) Ni/NiO-400, (c) Ni/NiO-450, (d) Ni/NiO-500 and (e) Ni/NiO-550.

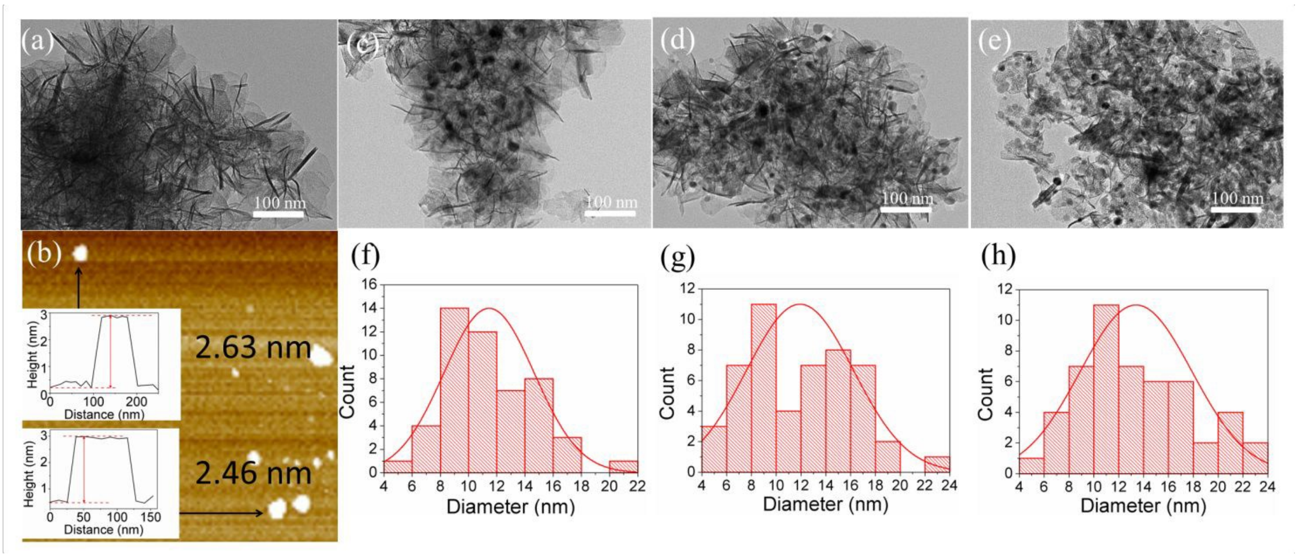

Fig. 3 TEM images of (a) pure NiO, (c) Ni/NiO-400, (d) Ni/NiO-450 and (e) Ni/NiO-500; (b) Atomic force microscopy (AFM) measurement result of thickness of pure NiO nanosheets. Statistical charts of Ni nanoparticles diameters of (f) Ni/NiO-400; (g) Ni/NiO-450 and (h) Ni/NiO-500.

sites with lower oxygen coordination (O_{II}).[33] The peak at 532.5 eV is mainly assigned to the surface-adsorbed oxygen species (O_{III}) on oxygen vacancies.[34] Furthermore, for Ni/NiO-450 and Ni/NiO-500, as shown in Figs. 4(b-c) and (e-f), the metallic state Ni^0 appears in addition to Ni^{2+} and Ni^{3+}, and the chemical states of O element are the same as those of pure NiO. At the

View Article Online
DOI: 10.1039/C9TA04487F

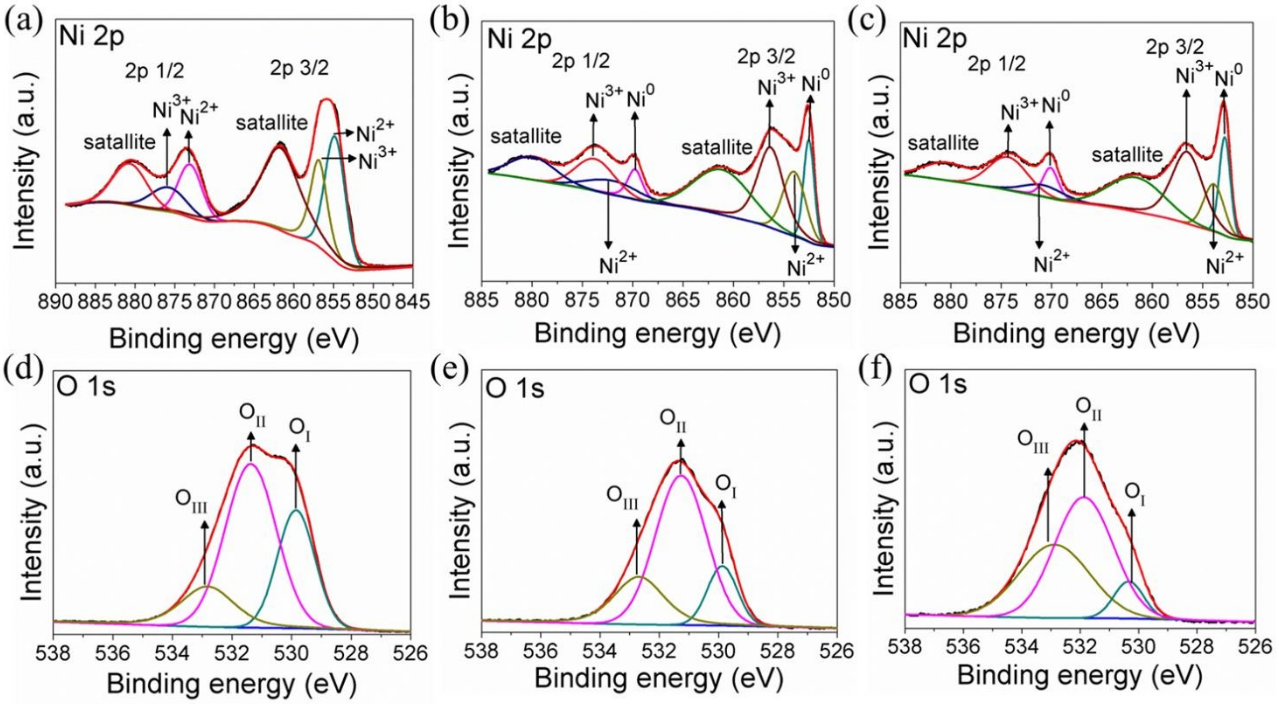

Fig. 4 XPS spectra of Ni 2p of (a) NiO, (b) Ni/NiO-450, (c) Ni/NiO-500 and O 1s of (d) NiO, (e) Ni/NiO-450, (f) Ni/NiO-500.

same time, the intensity ratio of O_{III}/O_{II} can qualitatively estimate the relative abundance of oxygen vacancies, and that the ratio clearly increasing with increases temperature. [35] Therefore, numerous vacancies have been verified to exist in the reduced samples.

In addition, the chemical binding energies of Ni^{2+} 2p3/2 of pure NiO, Ni/NiO-450 and Ni/NiO-500 are 854.8, 854.3 and 853.7 eV, respectively, while those of Ni^0 2p3/2 of Ni/NiO-450 and Ni/NiO-500 are 852.4 and 852.7 eV, respectively. That is, the chemical binding energy of Ni^{2+} shifts towards the higher energy direction while that of Ni^0 shifts towards the lower energy direction as the reduction temperature is increased. The lower binding energy of metallic Ni also indicates the decline of its electron density, which can lead to its d-band center shifting up and hence becoming a stronger adsorption for H_2. The shift in the opposite direction also indicates the strong interaction between Ni and NiO, which verifies the unique advantage of the *in situ* synthesis method. [36]

To determine the concentration of Ni in the obtained samples, H_2-temperature programmed reduction (TPR) tests were carried out. As shown in Fig. 5(a), for the pure NiO, hydrogen consumption peaks in the temperature range of 300–550 °C were observed, corresponding to the reduction of NiO to metallic nickel.[37] Meanwhile, similar hydrogen consumption peaks in the same temperature range were also observed for Ni/NiO-400, Ni/NiO-450 and Ni/NiO-500. The hydrogen consumption amounts of pure NiO, Ni/NiO-400, Ni/NiO-450 and Ni/NiO-500 are calculated to be about 0.63, 0.41, 0.34 and 0.22 mmol, respectively, according to the corresponding hydrogen consumption peak areas. Therefore, comparing the corresponding hydrogen consumption amounts with those of pure NiO, the Ni mole content of Ni/NiO-400, Ni/NiO-450 and Ni/NiO-500 are estimated to be 35%, 46% and 65%, respectively. To further verify the contents of Ni in each sample, temperature programmed oxidation (TPO) measurements were subsequently employed. As exhibited in Fig. 5(b), oxygen consumption peaks in the temperature range of 400-800 °C were observed, corresponding to the oxidation of metallic nickel to NiO. The oxygen consumption amounts of Ni/NiO-400, Ni/NiO-450 and Ni/NiO-500 are calculated to be approximately 0.16, 0.20 and 0.27 mmol while those for pure Ni are estimated to be about 0.43 mmol according to chemical reaction equations. Therefore, the Ni mole contents of Ni/NiO-400, Ni/NiO-450 and Ni/NiO-500 are calculated to be approximately 37%, 46% and 63% according to oxygen consumption amounts, respectively, which are in good

View Article Online
DOI: 10.1039/C9TA04487E

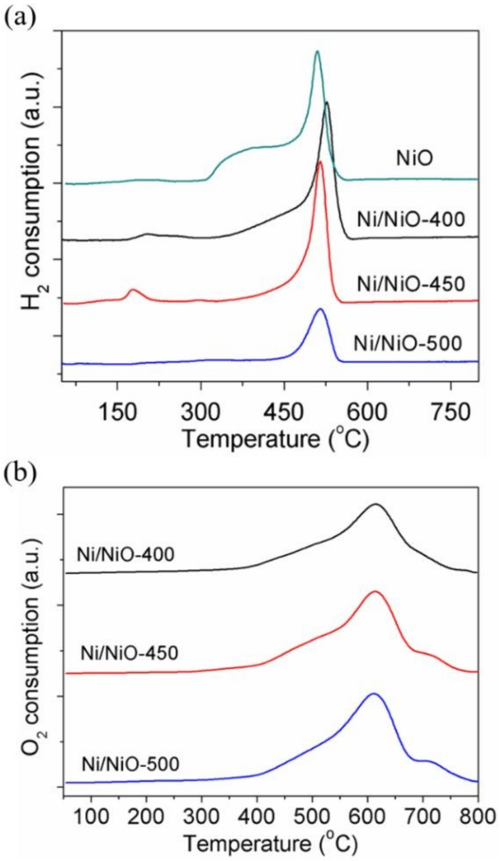

Fig. 5 (a) H_2-TPR spectra and (b) TPO spectra of Ni/NiO composite catalysts obtained at different reduction temperatures.

accordance with the results of H_2-TPR.

The specific surface area has been widely considered to be a vital factor to affect the performance of catalysts. Therefore, N_2 physical adsorption tests were then employed. It is shown in Fig. S6 that a typical IV N_2 adsorption isotherm with a H3 hysteresis loop is investigated at all of the profiles of the five samples, which is attributed to their mesoporous structures caused by the addition of $NaBH_4$ during synthesis producing numerous pores and in accordance with the previous reports.[38, 39] Additionally, the specific surface area of pure NiO is as large as approximately 173 $m^2 \cdot g^{-1}$, which benefits from its unique mesostructure of ultrathin nanosheets, as shown in Table 1. As the reduction temperature increases, the specific surface area shows a gradual decline, which is caused by the ultrathin and defect NiO that are reduced to Ni nanoparticles. The specific surface area of Ni/NiO-400, Ni/NiO-450 and Ni/NiO-500 still can be up to 127, 119 and 87 $m^2 \cdot g^{-1}$, respectively. However, there is a sharp decline for the Ni/NiO-550 with the specific surface area of only 0.16 $m^2 \cdot g^{-1}$, which is the result of the disappearance of NiO ultrathin nanosheets and aggregation of reduced Ni nanoparticles. Furthermore, as shown in Fig. S7, the largest weight change of NiO, Ni/NiO-400, Ni/NiO-450, Ni/NiO-500 and Ni/NiO-550 in water vapor adsorption curves is 30%, 29%, 27%, 26% and 4%, respectively. This also indicates that the specific surface area decreased as the temperature increased, and there is a sharp decline for Ni/NiO-550, which is in accordance with the results of the N_2 physical adsorption tests.[40] Meanwhile, the weight change of NiO is also larger than most reported materials at the same relative humidity, which further confirms its excellent adsorption performance with the unique structure of defect ultrathin nanosheets.[41]

Catalytic performances of the Ni/NiO catalysts: The samples were then applied to the hydrogenation of biomass platform molecule HFO to synthesize GBL. The catalytic performance of the as-prepared samples in the hydrogenation of HFO is listed in Table 2. Pure NiO exhibited almost no activity in the reaction.

Table 1 Specific surface area and pore structures of the Ni/NiO composite catalysts.

Sample	Specific surface area ($m^2\ g^{-1}$)	Pore size (nm)	Pore volume ($cm^3\ g^{-1}$)
NiO	173.16	18.31	0.83
Ni/NiO-400	127.38	20.05	0.70
Ni/NiO-450	119.56	21.50	0.68
Ni/NiO-500	87.31	25.72	0.40
Ni/NiO-550	0.16	—	—

Table 2 Catalytic performance of Ni/NiO composite catalysts for the hydrogenation of HFO.

Sample	Conversion (%)	Selectivity (%)	Yield (%)
NiO	—	—	—
Ni/NiO-400	38.8	81.1	31.5
Ni/NiO-450	45.7	87.8	40.1
Ni/NiO-500	95.6	90.5	86.6
Ni/NiO-550	0.5	—	—
NiO-thick nanosheets	—	—	—
Ni/NiO-250-thick nanosheets	2.0	—	—
Ni/NiO-300-thick nanosheets	5.7	35.2	2.0
Ni/NiO-400-thick nanosheets	37.9	70.2	26.6
Ni/C	—	—	—

View Article Online
DOI: 10.1039/C9TA04487F

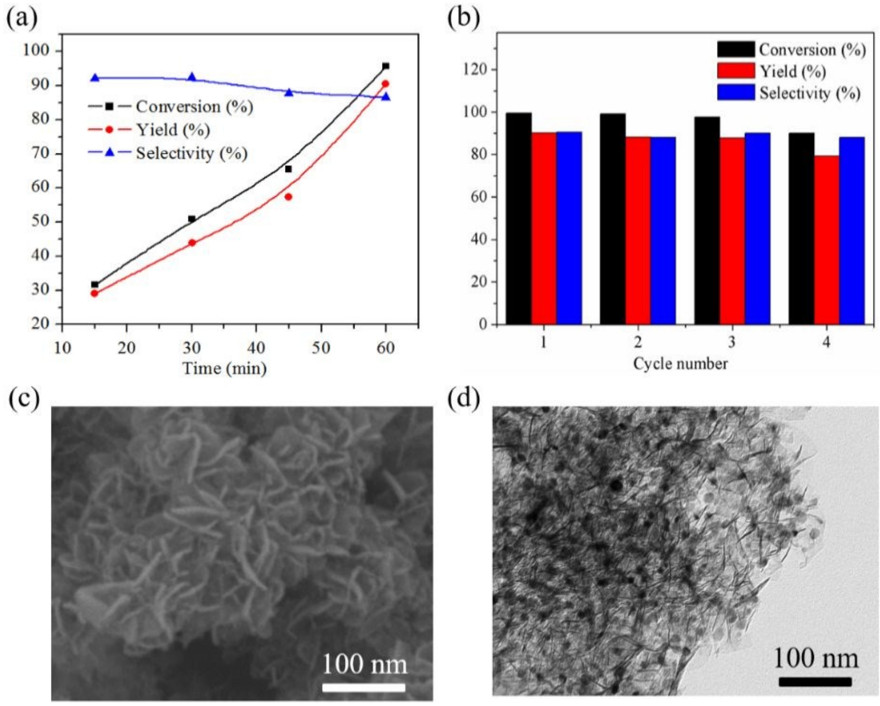

Fig. 6 (a) Variation in conversion and selectivity with reaction times for the HFO hydrogenation over the Ni/NiO-500 catalyst. (b) Recyclability of the Ni/NiO-500 catalyst for the hydrogenation of HFO. (c) SEM image and (d) TEM image of samples reclaimed after the fourth recycle.
Reaction conditions: catalysts 2.5 mg, HFO 0.4 g, H_2 3MPa, T 80 °C, time 60 min.

For the Ni/NiO-400, the conversion of HFO is 38.8% and the selectivity to GBL is 81.1%. For the Ni/NiO-450, the conversion and selectivity both increases up to 45.7% and 87.8%, respectively. For the Ni/NiO-500, the conversion increases to 95.6% and it has also the highest selectivity compared with the other samples. However, for Ni/NiO-550, the conversion decreases sharply to 0.5%. Moreover, the catalytic efficiency of samples with thick nanosheets was far lower than that of Ni/NiO-500, though the metallic Ni contents of Ni/NiO-300-thick nanosheets and Ni/NiO-400-thick nanosheets were much higher than those of Ni/NiO-500 (Fig. S8). The side products of 2(5H)-furanone (HFO) hydrogenation are mainly polymerization products, which cannot be identified through GC curves. Meanwhile, the simultaneous hydrogenation of C=O bond and the ring opening via C-O bond scission largely increase the difficulty of HFO selective hydrogenation to γ-butyrolactone (GBL). The typical GC curve is shown in Fig. S9 and the peaks at approximately 1.3, 3.3, 15.1 and 19.1 can be assigned to ethanol solvent, n-butanol internal standard, GBL and HFO, respectively. Fig. 6(a) shows the variation of HFO conversion and GBL selectivity with the reaction time in the hydrogenation of HFO for the Ni/NiO-500. The HFO conversion increases linearly to 95.6% within 60 min and the selectivity to GBL remains above 90.5% during the process. Wang *et al.* reported that Pt-Ni/SiO_2 showed both 95% conversion and 83% GBL selectivity, similarly Pt-Co/SiO_2 showed both 95% conversion and 79% GBL selectivity. [42] The catalytic performance of the present Ni/NiO-500 is comparable with those of Pt-Ni/SiO_2 and Pt-Co/SiO_2 catalysts reported in the literature. Furthermore, the conversion and selectivity obtained are similar or better than those bimetal (Pt-Ni, Pt-Co) catalysts in the short time periods (1 h). In addition, as shown in Figs. 6(b-d), the Ni/NiO-500 catalyst presented here exhibits excellent recyclability and stability. The conversion rate can still remain above 90% and the selectivity over 88% after the fourth cycle, and there is neither obvious damage on the flower-like morphologies nor the agglomeration of Ni nanoparticles.

View Article Online
DOI: 10.1039/C9TA04487F

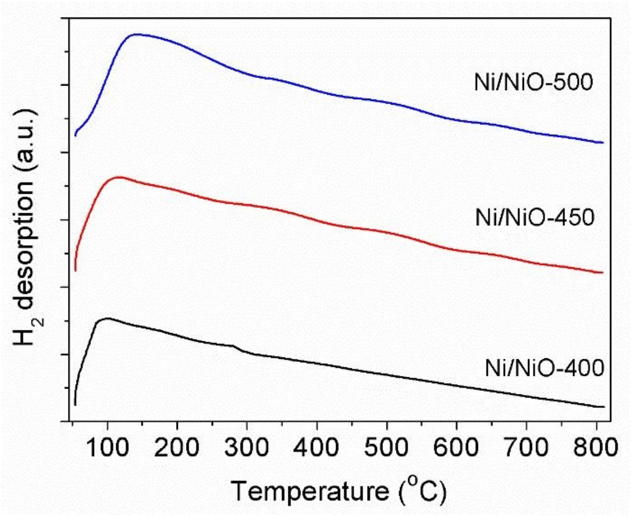

Fig. 7 H_2-TPD spectra of Ni/NiO composite catalysts obtained at different reduction temperatures.

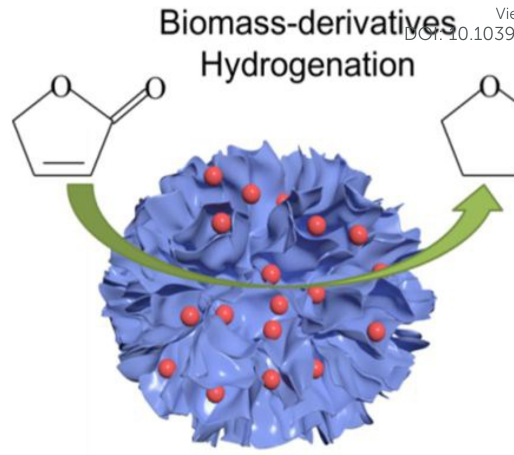

Scheme 1. The mechanism of the hydrogenation of HFO over the Ni/NiO composite catalysts.

To explore the origin of the superior performance of the Ni/NiO composites, H_2-temperature programmed desorption (TPD) measurements were then applied to observe the active sites in the reaction, as shown in Fig. 7. There is only one H_2 desorption peak, which is assigned to Ni for Ni/NiO-400, Ni/NiO-450 and Ni/NiO-500. Their H_2 desorption amounts were calculated to be 0.18, 0.20 and 0.24 mmol/g according to their corresponding peak areas, respectively. [43, 44] This indicates that the amount of hydrogen desorption increases with rising the reduction temperature. It is widely accepted that the greater the hydrogen desorption, the higher the catalytic activity is obtained. [45] Besides, according to the H_2 chemisorption results, the TOF values of Ni/NiO-400, Ni/NiO-450 and Ni/NiO-500 are 4105.8, 4352.4 and 7587.3 h^{-1}, respectively, indicating the improved performance of Ni/NiO-500 is led by not only the increasing Ni amounts, but also its enhanced intrinsic activities.

Based on the experimental results and the literature [46-49], it can be understood that the hydrogenation of HFO over the Ni/NiO composite catalysts involves the following crucial steps as shown in Scheme 1. First, hydrogen molecules are activated and dissociated by Ni nanoparticles while HFO could be captured by oxygen vacancies on the surface of ultrathin NiO nanosheets. Then, the active H species continue to react with HFO on the surface of pores existing in catalysts, which can be considered as nano-reactors for the hydrogenation of HFO. It is clear from the proposed mechanism that the activation and dissociation of hydrogen molecules as well as the adsorption of reactants are two key factors that affect the hydrogenation efficiency. Consequently, the extraordinary performance of Ni/NiO-500 can be attributed to the following reasons: (1) a substantial number of oxygen vacancies can largely reduce the energy barrier for the dissociation and activation of hydrogen, prompt the adsorption of HFO molecules through receiving their O atoms as well as result in high local hydrogen concentration on catalysts.[50] (2) Numerous Ni nanoparticles can effectively activate and dissociate hydrogen molecules. (3) The XPS measurement confirms the lower binding energy of metallic Ni, suggesting the decrease of its electron density leads to its d-band center shifting up and hence becoming a stronger adsorption for H_2.

To further verify the unique advantages of Ni/NiO heterojunctions with defect-rich ultrathin nanosheets and exploit their application areas, the samples were then applied to the hydrogenation of p-nitrophenol (PNP) and electrocatalytic nonenzymatic glucose sensing. (Details have been described in electronic supporting information.) Ni/NiO-500 also exhibits excellent performances in both reactions, which are even superior to most reported most reported noble metals. [51-68]

Conclusions

In conclusion, highly active Ni/NiO composite catalysts were successfully prepared by a simple *in situ* reduction method. The Ni/NiO-500 catalysts exhibit excellent performance in the selective hydrogenation of HFO to GBL, which is even superior to most reported noble metals. The excellent catalytic activities can be attributed to the synergism of geometric construction and electronic regulation. In particular, ultrathin NiO nanosheets contain plenty of surface defects and relatively large mesopores. Abundant defects can be helpful to the activation and dissociation of hydrogen, the adsorption of HFO molecules as well as the enhancement of local hydrogen concentration on catalysts, while the pores can be considered as nano-reactors for the hydrogenation. Numerous Ni nanoparticles could effectively activate and dissociate hydrogen molecules, which can be confirmed by decreasing binding energy of metallic Ni in the XPS measurement. In addition, the catalysts also display great performance in the hydrogenation of PNP and electrocatalytic properties for nonenzymatic glucose sensing, which further supports the promising application potential of

View Article Online
DOI: 10.1039/C9TA04487F

such catalysts with the unique mesostructures of Ni/NiO heterojunctions with defect-rich ultrathin nanosheets.

Conflicts of interest

There are no conflicts to declare.

Acknowledgements

We gratefully acknowledge the financial aid provided by the National Key Research and Development Program of China (2016YFB0701100), National Natural Science Foundation of China (51525101, 51402047, 51601032 and 21603212).

Notes and references

1 V. K. Das, Z. B. Shifrina and L. M. Bronstein, *J. Mater. Chem. A.*, 2017, **5**, 25131.

2 R. A. Sheldon, *Green Chem.*, 2014, **16**, 950.

3 D. M. Alonso, S. G. Wettstein and J. A. Dumesic, *Chem. Soc. Rev.*, 2012, **41**, 8075.

4 G. Q. Han, Y. H. Jin, R. A. Burgess, N. E. Dickenson, X. M. Cao and Y. J. Sun, *J. Am. Chem. Soc.*, 2017, **139**, 15584.

5 M. Besson, P. Gallezot and C. Pinel, *Chem. Rev.*, **2014**, 114, 1827.

6 A. Hashem and E. Kleinpeter, *Adv. Heterocycl. Chem.*, 2001, **81**, 107.

7 X. Li, Y. Y. Cui, X. L. Yang, W. L. Dai and K. N. Fan, Appl. Catal., A, 2013, **458**, 63.

8 G. Budroni and A. Corma, *J. Catal.*, 2008, **257**, 403.

9 K. Ceyda, C. Thomas and P. Joerg, *ChemCatChem,* 2018, **10**, 4931.

10 X. D. Li, X. X. C. Lan and T. F. Wang, Green Chem., 2016, 18, 638.

11 X. D. Li, Y. F. Li and T. F. Wang, *Catal. Today*, 2019, **319**, 93.

12 R. M. Bullock, Science, 2013, 342, 1054.

13 H. Yan, C. L. Su, J. He and W. Chen, J. Mater. Chem. A., 2018, 6, 8793.

14 L. Wang, E. Guan, J. Zhang, J. H. Yang, Y. H. Zhu, Y. Han, M. Yang, C. Cen, G. Fu, B. C. Gates and F. S. Xiao, Nat. Commun., 2018, 9(1362), 1

15 S. Manzeli, D. Ovchinnikov, D. Pasquier, O.V. Yazyev and A. Kis, *Nat. Rev. Mater.*, 2017, **2(17033)**, 1.

16 W. Zhang and K. Zhou, *Small*. 2017, **13(1700806)**, 1.

17 L. J. Lei, Z. W. Wu, H. Liu, Z. F. Qin, C. M. Chen, L. Luo, G. F. Wang, W. B. Fan, J. G. Wang, *J. Mater. Chem. A,* 2018, **6**, 9948.

18 B. Hammer and J. K. Nørskov, *Adv. Catal.,* 2000, **45**, 71.

19 B. I. Lundqvist, O. Gunnarsson, H. Hjelmberg and J. K. Nørskov, *Surf. Sci.,* 1979, **89**, 196.

20 H. L. Niu, J. H. Lu, J. J. Song, L. Pan, X. W. Zhang, L. Wang and J. J. Zhou, *Ind. Eng. Chem. Res.*, 2016, **55**, 8527.

21 W. W. Lin, H. Y. Cheng, L. M. He, Y. C. Yu and F. Y. Zhao, *J. Catal.*, 2013, **303**, 110.

22 F, Cao, F. Zhang, R. P. Deng, W. Hu, D. P. Liu, S. Y. Song and H. J. Zhang, *CrystEngComm*, 2011, **13**, 4903.

23 C. D. Lv, C. S. Yan, G. Chen, Y. Ding, J. X. Sun, Y. S. Zhou and G. H. Yu, *Angew. Chem. Int. Ed.,* 2018, **57**, 6073.

24 H. Fan, X. Huang, L. Shang, Y. T. Cao, Y. F. Zhao, L. Z. Wu, C. H. Tung, Y. D. Yin and T. R. Zhang, *Angew. Chem. Int. Ed.,* 2016, **55**, 2167.

25 M. Xu, S. He, H. Chen, G. Q. Cui, L. R. Zheng, B. Wang and M. Wei, *ACS Catal,* 2017, **7**, 7600.

26 Y. Z. Su, Q. Z. Xu, G. F. Chen, H. Cheng, N. Li and Z. Q. Liu, *Elecrochim. Acta,* 2015, **174**, 1216.

27 X. L. Xu, L. Li, J. Huang, X. Z. Fang, W. M. Liu, N. Zhang, H. M. Wang and X. Wang, *ACS Catal.,* 2018, **8**, 8033.

28 J. H. Li, C. C. Wang, C. J. Huang, Y. F. Sun, W. Z. Weng and H. L. Wan, *Appl. Catal. A-Gen.,* 2010, **382**, 99.

29 B. Zhao, X. K. Ke, J. H. Bao, C. L. Wang, L. Dong, Y. W. Chen, H. L. Chen, *J. Phys. Chem. C,* 2009,**113**, 14440.

30 J. Zhang, X. Wu, W. C. Cheong, W. X. Chen, R. Lin, J. Li, L. R. Zheng, W. S. Yan, L. Gu, C. Chen, Q. Peng, D. S. Wang and Y. D. Li, *Nat. Commun.,* 2018, **9(1002)**, 1.

31 M. Stoyanova, P. Konova, P. Nikolov, A. Naydenov, S. Christoskova and D. Mehandjiev, *Chem. Eng. J.,* 2016, **122**, 41.

32 N. S. Mclntyre and M. G. Cook, *Anal. Chem.*, 1975, **47**, 2208.

33 J. Bao, X. D. Zhang, B. Fan, J. J. Zhang, M. Zhou, W. L. Yang, X. Hu, H. Wang, B. C. Pan and Y. Xie, *Angew. Chem. Int. Ed.,* 2015, **54**, 7399.

34 F. Y. Cheng, T. R. Zhang, Y. Zhang, J. Du, X. P. Han and J. Chen, *Angew. Chem. Int. Ed.,* 2013, **52**, 2474.

35 Q. Hu, L. Yang, G. L. Fan and F. Li, *J. Catal.,* 2016, **340**, 184.

36 H. Wang, C. L. Chen, Y. X. Zhang, L. X. Peng, S. Ma, T. Yang, H. H. Guo, Z. D. Zhang, D. S. Su and J. Zhang, *Nat. Commun.,* 2015, **6(7181)**, 1.

37 X. L. Xu, L. Li, J. Huang, H. Jin, X. Z. Fang, W. M. Liu, N. Zhang, H. M. Wang and X. Wang, *ACS Catal.,* 2018, **8**, 8033.

38 Y. N. Wang, J. M. Wang, R. P. Deng, S. W. Xv, X. Lv, J. Zhou, S. Li, F. Cao and G. W. Qin, *Mater. Res. Bull.,* 2018, **107**, 94.

39 P. Y. Gong, B. S. Li, X. L. Kong, J. J. Liu and S. L. Zuo, *Appl. Surf. Sci.*, 2017, **423**, 433.

40 H. Maeda and E. H. Ishida, *Ceram. Int.,* 2009, **35**, 987.

41 F. Cao, D. Y. Li, R. P. Deng, L. J. Huang, D. C. Pan, J. M. Wang, S. Li and G. W. Qin, *RSC Adv.,* 2015, **5**, 84587.

42 X. D. Li, W. M. Wan, S. Kattel, J. G. Chen and T. F. Wang, *J. Catal.,* 2016, **344**, 148.

43 W. W. Lin, H. Y. Cheng, L. M. He, Y. C. Yu and F. Y. Zhao, *J. Catal.,* 2013, **303**, 110.

44 K. Xiong, G. L. Zhou, H. D. Zhang, Y. Shen, X. M. Zhang, Y. H. Zhang and J. L. Li, *J. Mater. Chem. A,* 2018, **6**, 15510.

45 Y. X. Liu, J. X. Chen and J. Y. Zhang, *Chin. J. Chem. Eng.*, 2007, **15**, 63.

46 L. Ye, X. P. Duan, S. Wu, T. S. Wu, Y. X. Zhao, A. W. Robertson, H. L. Chou, J. W. Zheng, T. Ayvalı, S. Day, C. Tang, Y. L. Soo, Y. Z. Yuan, and S. C. E. Tsang, *Nat. Commun.*, 2019, **10**, 1.

47 L. H. Zhu, S. Y. Shan, V. Petkov, W. W. Hu, A. Kroner, J. B. Zheng, C. L. Yu, N. W. Zhang, Y. H. Li, R. Luque, C. J. Zhong, H. Q. Ye, Z. Q. Yang and B. H. Chen, *J. Mater. Chem. A,* 2017, **5**, 7869.

48 C. Lin, G. H. Wu, H. Q. Li, Y. M. Geng, G. Xie, J. H. Yang, B. Liu and J. Jin, *Nanoscale*, 2017, **9**, 1834.

49 B. F. Chen, F. B. Li and G. Q. Yuan, *RSC Adv*., 2017, **7**, 21145.

50 J. A. Rodriguez, J. C. Hanson, A. I. Frenkel, J. Y. Kim and M. Pérez, *J. Am. Chem. Soc.,* 2002, **124**, 346.

51 X. Wang, R. Y. Cao, S. W. Zhang, P. Y. Hou, R. X. Han, M. H. Shao and X. J. Xu, *J. Mater. Chem. A,* 2017, **5**, 23999.

52 D. D. Jia, H. Y. Gao, W. J. Dong, S. Fan, R. Dang and G. Wang, *ACS Appl. Mater. Interfaces,* 2017, **9**, 20476.

53 J. W. Xia, G. Y. He, L. L. Zhang, X. Q. Sun and X. Wang, *Appl. Catal. B: Environ.,* 2016, **180**, 408.

54 J. W. Wu, W. Liu, X. Xiang, K. Sun, F. H. Liu, C. Cai, S. B. Han, Y. Y. Xie, S. A. Li and X. T. Zu, *Carbon*, 2017, **117**, 192.

55 Q. Liu, Y. R. Xu, A. J. Wang and J. J. Feng, *RSC Adv.,* 2015, **5**, 96028.

56 C. M. Fan, L. F. Zhang, S. S. Wang, D. H. Wang, L. Q. Lu and A. W. Xu, *Nanoscale*, 2012, **4**, 6835.

View Article Online
DOI: 10.1039/C9TA04487F

57 X. Gao, H. Zhao, Y. G. Liu, Z. P. Ren, C.P. Lin, J. L. Tao and Y. P. Zhai, *Mater. Chem. Phys.,* 2019, **222**, 391.
58 X. Wang, R. Y. Cao, P. Y. Hou, R. X. Han, M. H. Shao and X. J. Xu, *J. Mater. Chem. A,* 2017, **5**, 23999.
59 X. Y. Li, C. M. Zeng, J. Jiang and L. H. Ai, *J. Mater. Chem. A.,* 2016, **4**, 7476.
60 K. Yang, Y. Yan, H. Y. Wang, Z. X. Sun, W. Chen, H. T. Kang, Y. Han, W. Q. Zhang, X. H. Sun and Z. X. Li, *Nanoscale,* 2018, **10**, 17647.
61 B. K. Barman and K. K. Nanda, *ACS Sustainable Chem. Eng.,* 2018, **6**, 12736.
62 P. Zhang, X. Y. Yang, H. L. Peng, D. Liu, J. F. Wei and J. Z. Gui, *Catal. Commun.,* 2017, **100**, 214.
63 Y. Liang, Z. Chen, W. Yao, P. Y. Wang, S. J. Yu and X. K. Wang, *Langmuir,* 2017, **33**, 7606.
64 W. Fang, Y. C. Deng, L. Tang, G. M. Zeng, Y. Y. Zhou, X. Xie, J. J. Wang, Y. Wang and J. J. Wang, *J. Colloid Interf. Sci.,* 2017, **490**, 834.
65 R. Ojani, J. B. Raoof and B. Norouzi, *J. Solid State Electrochem*, 2011, **15**, 1139.
66 L. Wang, Y. Z. Xie, C. T. Wei, X. P. Lu, X. Li and Y. H. Song, *Electrochim. Acta,* 2015, **174**, 846.
67 K. K. Lee, P. Y. Loh, C. H. Sow and W. S. Chim, *Electrochem. Comm.*, 2012, **20**, 128.
68 M. Q. Guo, H. S. Hong, X. N. Tang, H. D. Fang and X. H. Xu, Electrochim. Acta, 2012, 63, 1.